Title

1,3-Dipolar Cycloaddition Reactions of Low-Valent Rhodium and Iridium Complexes with Arylnitrile N-Oxides

Journal

The Journal of Organic Chemistry, 82(10)

ISSN

0022-3263

Authors

Ugur, Ilke
Cinar, Sesil Agopcan
Dedeoglu, Burcu
et al.

Publication Date

2017-05-19

DOI

10.1021/acs.joc.7b00282

Peer reviewed

HHS Public Access

Author manuscript

J Org Chem. Author manuscript; available in PMC 2017 November 09.

Published in final edited form as:

J Org Chem. 2017 May 19; 82(10): 5096–5101. doi:10.1021/acs.joc.7b00282.

1,3-Dipolar Cycloaddition Reactions of Low-Valent Rhodium and Iridium Complexes with Arylnitrile *N*-Oxides

Ilke Ugur[†,‡], **Sesil Agopcan Cinar**[†], **Burcu Dedeoglu**[§], **Viktorya Aviyente**[†], **M. Frederick Hawthorne**[‖], **Peng Liu**[‡,¶,iD], **Fang Liu**[‡], **K. N. Houk**[*,‡,iD], and **Gonzalo Jiménez-Osés**[*,⊥,iD]

[†]Department of Chemistry, Bogazici University, Bebek, Istanbul 34342, Turkey

[‡]Department of Chemistry and Biochemistry, University of California, Los Angeles, Los Angeles, California 90095-1569, United States

[§]Foundations Development Directorate, Sabancı University, Tuzla-Orhanlı, Istanbul 34956, Turkey

[‖]International Institute of Nano and Molecular Medicine, University of Missouri, Columbia, Missouri 65211-3450, United States

[⊥]Departamento de Química, Centro de Investigación en Síntesis Química, Universidad de La Rioja, 26006 Logroño, La Rioja, Spain

Abstract

The reactions between low-valent Rh(I) and Ir(I) metal–carbonyl complexes and arylnitrile oxides possess the electronic and structural features of 1,3-dipolar cycloadditions. Density functional theory (DFT) calculations on these reactions, involving both cyclopentadienyl and carboranyl ligands on the metal carbonyl, explain the ease of the chemical processes and the stabilities of the resulting metallaisoxazolin-5-ones. The metal–carbonyl bond has partial double bond character according to the Wiberg index calculated through NBO analysis, and so the reaction can be considered a normal 1,3-dipolar cycloaddition involving M═C bonds. The rates of formation of the metallacycloadducts are controlled by distortion energy, analogous to their organic counterparts. The superior ability of anionic Ir complexes to share their electron density and accommodate higher oxidation states explains their calculated higher reactivity toward cycloaddition, as compared to Rh analogues.

Graphical abstract

[*]**Corresponding Authors**. houk@chem.ucla.edu, gonzalo.jimenez@unirioja.es.

ORCID

Peng Liu: 0000-0002-8188-632X

K. N. Houk: 0000-0002-8387-5261

Gonzalo Jiménez-Osés: 0000-0003-0105-4337

[¶]**Present Address**

Department of Chemistry, University of Pittsburgh, Pittsburgh, Pennsylvania 15260, United States.

ASSOCIATED CONTENT

Supporting Information

The Supporting Information is available free of charge on the ACS Publications website at DOI: 10.1021/acs.joc.7b00282.

Additional figures, Cartesian coordinates, electronic energies, entropies, enthalpies, Gibbs free energies, and lowest frequencies of the calculated structures (PDF)

The authors declare no competing financial interest.

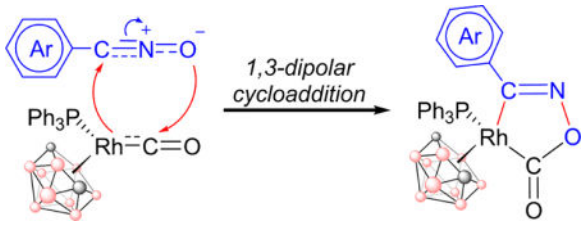

INTRODUCTION

Numerous 1,3-dipolar cycloaddition reactions have been carried out since the discovery of diazoacetic ester by Curtius in 1883[1] and the establishment of the general concept of 1,3-dipolar cycloadditions by Rolf Huisgen.[2] Interest in these reactions has exploded, because of their many uses including biological applications.[3,4] The mechanisms of 1,3-dipolar cycloadditions have been extensively studied computationally, including the metal catalyzed variants.[5–7] Nitrile oxides undergo cycloadditions with alkenes, alkynes, and carbon-heteroatom multiple bonds. Remarkably, cycloadditions to metal–carbonyl bonds occur with maintenance of the metal–carbon (M–C) bond.[8,9] Hawthorne and co-workers reported the reaction between *m*-fluorobenzonitrile *N*-oxide and rhodacarborane anion $[Rh\text{-}(PPh_3)(CO)(C_2B_9H_{11})]^-$ as the first 1,3-dipolar addition to a metal–carbon bond (Figure 1).[10]

Subsequently, the same group synthesized several five-membered metallacycles via 1,3-dipolar cycloaddition reactions of arylnitrile *N*-oxides to metallacarborane carbonyls with either Rh or Ir as metals.[11,12] The $(C_2B_9H_{11})^{2-}$ ligand has been used to form sandwich-type complexes resulting from the ligation of two separate carborane anions to the metal center (commonly Ni or Co).[13–16]

The scientific interest of boron-rich chemical compounds has increased as they have been successfully used in polymers and pharmaceuticals. The discovery of the dodecaborate anion $(B_{12}H_{12})^{2-}$ by Hawthorne and co-workers[17] and further applications of its derivatives expanded the usage of boron clusters. Hawthorne's discovery of the use of carboranes $(C_2B_9H_{11})$ as ligands in metal-sandwich complexes led to the preparation of several metallacarboranes[18] for applications in medicinal chemistry,[19] olefin polymerization,[20] and nuclear waste remediation.[21,22]

We have used several types of density functional theory (DFT) methods to study the 1,3-dipolar cycloaddition reactions of low valent metallacarborane complexes with four distinct arylnitrile *N*-oxide dipoles to understand the nature of this reaction and the substituent effects on rates and the stabilities of the metallacyclic products. The cycloadditions of low valent metal cyclopentadienyl complexes, the isolobal counterpart of the carborane,[23] were also studied. Different *meta* and *para* substituted arylnitrile *N*-oxides were studied as 1,3-dipoles (**1a–d** in Figure 2); rhodium– and iridium–carbonyl complexes of carborane (dicarbollide) and cyclopentadienyl constituted dipolarophiles (**2a–d** in Figure 2). NBO-based Wiberg bond order indices, root-mean-square deviations of computed versus experimental geometries, and bonding distances in reactants and products were used to characterize these species.

Distortion/interaction energies and thermodynamical contributions to the reaction energies were computed to better understand the origins of reactivity and mechanisms of reactions of the modeled metallacyclic complexes.

Computational Details

Geometry optimizations were performed using density functional theory (DFT) with the B3LYP[24] functional. Grimme's dispersion correction (D3) was included during geometry optimizations.[25] The Stuttgart/Dresden effective core potential (SDD) was used for Rh and Ir, while the rest of the atoms were treated with the 6-31G(d) basis set. A similar basis set augmented with diffuse functions, i.e., 6-31+G(d), was used in selected cases with comparative purposes (see Supporting Information). Also for selected cases, the influence of solvent effects in reactions involving ionic species was evaluated implicitly through the SMD polarizable continuum model[26] using tetrahydrofuran as a solvent. All stationary points were characterized by a frequency analysis from which thermal corrections have also been obtained at 298.15 K. Local minima and first order saddle points were identified by the number of imaginary vibrational frequencies. Intrinsic reaction coordinate (IRC)[27] calculations were performed on the transition structures to determine the connectivity with the corresponding product and reactant. Single point energy calculations were performed using the M06 functional[28] with the same basis set. Wiberg indices[29] were calculated based on the natural bond orbital (NBO) analysis.[30] Calculations were carried out with Gaussian 09.[31] Products and transition structures are named according to the 1,3-dipolarophile and the dipole involved, for instance, **1a–2a** and **ts-1a-2a** denote products and the transition structure involving reaction of dipole **1a** with the dipolarophile **2a**, respectively. Graphics were generated with Claude Legault's CYLView.[32]

RESULTS AND DISCUSSION

Structural Features of the Cycloadducts: Effect of Dispersion Correction (D3)

All the reactants, transition states, and products were optimized using both B3LYP and dispersion corrected B3LYP-D3 functionals. The geometrical features of products **1d–2a** were analyzed and compared with the available X-ray structures.[11] Distances are in agreement with the experimental data, with a root-mean-square deviation (RMSD) of 0.03 and 0.02 Å with B3LYP and B3LYP-D3 calculations, respectively (the list of the distances is given in the Supporting Information, Table S1). The differences between the two theory methods and comparisons with the experimental structure were also evaluated (Figure S1). For B3LYP calculations, higher deviations from experiment were found for the distances related to the Rh atom. These distances were improved using D3 corrections. The calculated angles and dihedrals were also analyzed (Figure S2). None of the angles were significantly affected by including dispersion corrections (the maximum difference between B3LYP and B3LYP-D3 is ~5°). This observation is also valid for most of the calculated dihedrals. Exceptionally, the dihedral around the aryl group (Rh–C_{29}–C_{30}–C_{33}) changed from −153° to −125° when dispersion corrections were added (Figure 3 for B3LYP-D3 and Figure S3 for B3LYP structures). This smaller dihedral yields a closer orientation of the aryl group to one of the phenyl ligands on Rh (Figure 3).

The center to center distances of the fluorobenzene group of dipole, **1d**, and two phenyl ligands of Rh of dipolarophile, **2a**, were also measured (Figure 3, right panel). These three aryl groups (one from **1d** and two from **2a**) are packed in a conformation forming an aromatic cyclic trimer, related to the arrangement observed in small benzene clusters in vacuum (with a total interaction energy more than 5 kcal mol^{-1}).[33–36] Cyclic trimers are also characterized as commonly occurring motifs in proteins, and they are suggested to be one of the factors contributing to stabilization of protein tertiary structures.[37] For the structure optimized with B3LYP-D3, the distances between the centers of the aryl groups are shorter (4.5, 4.8, and 5.2 Å) and closer to the benzene trimer reference value of 4.7 Å.[38] As discussed above, when dispersion corrections (D3) are included, the fluorophenyl group of dipole **1d** gets closer to the phenyl ligands of Rh (smaller dihedral value at Rh–C_{29}–C_{30}–C_{33} of −125°), resulting in a better packing of the cyclic trimer.

Benchmarking the Reaction Energetics

As introduced in the previous section, the calculated structure of the **1d–2a** adduct is improved by including the D3 dispersion correction. This improvement was also reflected in the reaction free energy (ΔG_r) which became more negative: −24.7 kcal mol^{-1} with B3LYP-D3 versus −7.3 kcal mol^{-1} with B3LYP. A similar increase in ΔG_r (~17 kcal mol^{-1}) by including dispersion was observed for all the studied adducts (Table S2). The same trend is also valid for the computed activation energy ($\Delta G^{\ddagger}$) for the cycloaddition reactions, decreasing from an average of ~25 kcal mol^{-1} with B3LYP to an average of ~8 kcal mol^{-1} with B3LYP-D3. However, the barriers calculated with B3LYP and B3LYP-D3 are over and underestimated, respectively, considering the mild experimental conditions needed to complete the reactions (~5 h at 20–25 °C).[10,17] In an attempt to improve our energetic data we performed single point energy calculations with the M06 and M06-D3 methods on the B3LYP-D3 optimized geometries, which were closer to the experimental ones. The M06 functional was previously shown to reproduce accurate energy results for transition metal bearing complexes for other systems.[28,39,40] The average value for the activation barriers was calculated to be ~15 kcal mol^{-1} with M06, which is more consistent with the experimental conditions. Notably, adding dispersion corrections (D3) to M06 yielded nearly identical results as B3LYP-D3, again underestimating reaction barriers (Table S2). Hence, we will use the M06//B3LYP-D3 results throughout the manuscript as they are more compatible with the experimental data. Regarding the basis sets, adding diffuse functions during optimization, which might be convenient to correctly describe anionic species, raises the energies of the stationary points of the reactions **2a + 1a** and **2b + 1a** by 7–9 kcal mol^{-1} (Supporting Information), and convergence problems were experienced. Similarly, including solvent effects (tetrahydrofuran) increases both the activation and reaction energies for the same reactions by 10–12 kcal mol^{-1} (Supporting Information). However, it should be noted that although there are major quantitative energetic differences within the results obtained by these functionals, the trend in the reactivities, which is detailed below, is correctly represented by all of these methods (Table S2 and Table 1).

Low Valent Metal–Carbonyl Complexes as Dipolarophiles

The computed Gibbs free energies for the reactions between dipolarophile **2a** and all 1,3-dipoles studied (**1a–d**) are represented graphically (Figure 4). For all the modeled systems,

the activation energies ($\Delta G^{\ddagger}$) range from 11 to 13 kcal mol^{-1}, and the exergonicities of the reactions ((ΔG_r) range from −15 to −19 kcal mol^{-1} (Figure 4 and Table 1). Substitution on the aryl dipoles (**1a–d**) has only a small effect on both $\Delta G^{\ddagger}$ and ΔG_r, only 1–3 kcal mol^{-1} between the highest (**1a–2a**) and lowest (**1b–2a**) values.

The calculated energies indicate a facile reaction between the low valent metal–carbonyl complex **2a** and nitrile oxides (**1a–1d**) leading to stable cycloadducts in which the metal center is oxidized from Rh(I)/Ir(I) to Rh(III)/Ir(III). Conventional 1,3-dipolar cycloaddition reactions occur to an alkene or alkyne of the dipolarophile. Metal–carbonyl complexes have been suggested to be plausible dipolarophile candidates exhibiting back bonding from carbonyl to metal, which results in multiple bond character. To corroborate this hypothesis, we have investigated the bonding character of the metal–carbonyl complex **2a** and the product of its reaction with the dipole **1d** by natural bond orbital (NBO) analysis. The calculated Wiberg indices of the bonds of interest for the reactants (**2a** and **1d**), transition state (**ts-1d-2a**), and product (**1d–2a**) are given in Table 2. For comparison, the Wiberg indices of the reaction between **1d** and a prototypical dipolarophile (ethylene) were also calculated (Table 2, numbers in parentheses).

In the reactant **2a**, the Wiberg index for the bond Rh–C_2 has a value of 1.2. This value indicates a partial double bond, given that the Wiberg index of the C═C double bond in ethylene is 2.0 using the same localization scheme. The conversion of the partial double bond (1.2) to a single bond occurs in the transition state, as the value drops to 1.1. The final value of the corresponding bond is 0.7, indicating a weaker bond compared to its isolobal ethylene counterpart (1.0). Throughout the reaction, a decrease of 0.5 is observed for both the C1–N1 and the N1–O1 bond indices. In the final product, both of these two bonds have similar character with respect to the reaction with ethylene. The newly formed C_2–O_1 and Rh–C_1 bonds have single bond character, although the Rh–C_1 bond is weaker (0.7) compared to the C–C_1 bond in the ethylene-**1d** adduct (1.0).

Overall, the metal–carbon bond (Rh–C_2) transforms from a partial double to a partial single bond, similarly to a conventional organic 1,3-dipolar cycloaddition reaction. The bonds between the metal center and the carbon atoms (C_1 and C_2) are equally strong, but they both involve less electron-sharing than a conventional C–C single bond.

Reactivity of Different Low Valent Metal–Carbonyl Complexes

The reactivities of the various metal carbonyls were analyzed by considering three structural effects on either the dipole or the dipolarophile: (1) the effect of the halogen substitution (F or Cl) on the arylnitrile oxides (**1a–d**); (2) the effect of the metal center (Rh in **2a**/**2c** or Ir in **2b**/**2d**); (3) the effect of the ligand (carborane in **2a**/**2b** or cyclopentadienyl in **2c**/**2d**). Among these three structural differences, substitution on the arylnitrile has a very small impact on the calculated activation or reaction energies (a maximum of 3 kcal mol^{-1} difference, Table 1). Chloro substitution on the *para* position (**1b**) yields the lowest activation barrier ($\Delta G^{\ddagger}$) for three cases, **2a** being an exception. The halogen substituent effect is generally quite small.

Changing the metal center from Rh (**2a**/**2c**) to Ir (**2b**/**2d**) has a negligible influence on the activation barriers, with a difference smaller than 1 kcal mol^{-1} when analogous systems are compared. However, Ir complexes are remarkably more stable (~8 kcal mol^{-1}) than the Rh counterparts, due to the known greater ability of third-row transition metals to stabilize higher oxidation states with respect to their second-row counterparts.

The choice of the ligand on the metal has the greatest impact on the reaction barriers. Thus, substituting the cyclopentadienyl (charge −1) by the carboranyl ligand (charge −2) reduces the activation energy up to 5 kcal mol^{-1}, comparing **2c** to **2a** (or **2d** to **2b**). Similarly, the reaction energies become more favorable by approximately 4–7 kcal/mol^{-1}. This is due to the higher electron richness and nucleophilic character of the anionic carboranyl complexes with respect to the neutral cyclopentadienyl analogues. Also, anionic species are known to accommodate higher oxidation states better than neutral ones. Hence, the combination of dipole **1b** (bearing a *para*-Cl substitution) and dipolarophile **2b** (Ir center coordinated to a carboranyl ligand) yields the most exergonic reaction (ΔG_r = −26.7 kcal mol^{-1}) with one of the smallest activation barriers ($\Delta G^{\ddagger}$ = 12.6 kcal mol^{-1}) in this series.

The enthalpic (ΔH) and entropic ($-T{\cdot}\Delta S$) contributions to the reaction energies are also reported in Table 1. As expected, the entropic contribution was found to be essentially constant ($-T{\cdot}\Delta S$ ~ 18–19 kcal mol^{-1}, typical for bimolecular processes), and the differences in the product stabilities are mostly correlated with the reaction enthalpy.

Charge transfer (CT) is found to correlate only with the aryl ring substitution at the dipole: CT increases slightly from unsubstituted (0.16 electrons in reactions involving **1a**) to *para*-substituted systems (0.18–0.19 electrons in reactions with **1b** and **1c**). The greatest charge transfer was consistently measured for the reactions involving *meta*-F-substituted **1d** (0.23 electrons).

Distortion/Interaction Analysis

To gain a deeper insight on the reactivity of the different systems, a distortion/interaction analysis was performed. The energy required to distort the reactants to their transition state geometries is described as the distortion energy. The interaction energy is the energy of interaction of the two distorted reactants in the transition state geometry. The sum of these two terms is the activation barrier of the reaction. The activation barriers for the formation of a wide range 1,3-dipolar cycloadducts were found previously to be correlated with the corresponding distortion energies.[41–51] A linear correlation between activation and distortion energies has been previously shown by Houk and co-workers for a set of prototypical 1,3-dipolar cycloaddition reactions using highly accurate methods.[42,51] Figure 5 gives the distortion and interaction energies calculated here, compared to activation energies. This analysis uses electronic energies rather than free energies. In the present study, the distortion energies (ΔE_d) are found to be linearly correlated with activation barriers ($\Delta E^{\ddagger}$), with a correlation coefficient (R^2) of 0.864 (Figure 5, left panel). As in simpler reactions, the energy required to distort the dipoles and the dipolarophiles into the transition state geometry controls the reaction barrier. On the other hand, interaction energies (ΔE_i) correlate poorly with activation barriers (R^2 = 0.526, Figure 5, right panel).

Among the different 1,3-dipoles, the transition structures derived from unsubstituted **1a** and *para*-Cl-substituted **1b** consistently show the highest and lowest distortion energies, respectively. Metal substitution, on the other hand, has the smallest and less consistent effect on distortion energies and consequently on activation barriers (although it has a dramatic effect on the stability of the cycloadducts, as discussed above).

By far, the strongest effect on distortion energy is due to the ligand bound to the metal center; the accelerating effect shown by the doubly charged carboranyl anion translates into earlier, and thus less distorted and lower in energy, transition states (Figure 5 squares and Figure 6 top) than their cyclopentadienyl counterparts (Figure 5 circles and Figure 6 bottom). This is clearly shown by the significantly longer forming bonds and more linear 1,3-dipole bending angles in **ts-1d-2a/b** (Rh/Ir–C_1 ~ 2.8 Å; C_2–O_1 ~ 2.8–2.9 Å; C_1–N_1–O_1 ~ 150°) compared to those in **ts-1d-2c/d** (Rh/Ir–C_1 ~ 2.6–2.7 Å; C_2–O_1 ~ 2.6–2.7 Å; C_1–N_1–O_1 ~ 145°).

In summary, anionic, electron-rich metal carbonyls have a higher propensity to react with 1,3-dipoles through earlier, less distorted transition structures (i.e., are more nucleophilic) than their neutral analogues.

CONCLUSIONS

We modeled the 1,3-dipolar cycloaddition reactions of arylnitrile *N*-oxides with low-valent metal carbonyl complexes. The partial double bond character of the metal–carbonyl bond originating from the M═C═O resonance Lewis structure, as well as the ability of the Rh/Ir atoms to increase their coordination number from five to six, and the alteration of the metal–carbon bond character from a partial double bond to a single bond allows these complexes to react as dipolarophiles.

The cycloadduct products are stabilized by the formation of a compact aromatic cyclic trimer between the PPh_3 ligands on the metal and aromatic ring on the 1,3-dipoles. While the interaction energy between the reactant species is almost constant for all the studied systems, the differences in the activation barriers are determined by the distinct distortion energies of each type of complex. Analogous to their organic counterparts, the reactivities of these metal complexes increase as the energies to distort the reactant to their transition state geometries decrease. In our model set, the substitution of the cyclopentadienyl ligand by carboranyl produces more nucleophilic anionic complexes resulting in a major reduction of their distortion energies. On the other hand, Ir(I) complexes yield much more stable Ir(III) cycloadducts than their Rh analogues, due to the higher capacity of third-row transition metals to stabilize higher oxidation states, particularly when forming anionic species. Through these studies we scrutinized the sources of reactivity of metal carbonyls toward 1,3-cycloaddition with aryl arylnitrile *N*-oxides, whose cyclic adducts (metallaisoxazolin-5-ones) are capable to undergo thermal decomposition of CO_2.[52] Our computational studies on these processes are the subject of a follow-up report.

Supplementary Material

Refer to Web version on PubMed Central for supplementary material.

Acknowledgments

We are grateful to the Bogazici University Research Funds and the NIH-FIRCA project (R03TW007177), as well as the National Institute of General Medical Sciences, National Institutes of Health (GM109078 to K.N.H.) and D.G.I. MINECO/FEDER (projects CTQ2015-70524-R and RYC-2013-14706 to G.J.O.). Computing resources used in this work were provided by the TUBITAK ULAKBIM High Performance and Grid Computing Center, the National Center for High Performance Computing (UHeM) under grant number 11062010, CESGA, UR (Beronia cluster), and UCLA Academic Technology Services/Institute for Digital Research and Education. We would like to thank Dr. Antoine Marion for his helpful comments and providing the python code for structural analysis.

References

1. Curtius T. Ber. Dtsch. Chem. Ges. 1883; 16:2230–2231.
2. Huisgen R. Angew. Chem. Int. Ed. Engl. 1963; 2:565–598.
3. Kamber DN, Nazarova LA, Liang Y, Lopez SA, Patterson DM, Shih H-W, Houk KN, Prescher JA. J. Am. Chem. Soc. 2013; 135:13680–13683. [PubMed: 24000889]
4. Kamber DN, Liang Y, Blizzard RJ, Liu F, Mehl RA, Houk KN, Prescher JA. J. Am. Chem. Soc. 2015; 137:8388–8391. [PubMed: 26084312]
5. Gothelf KV, Jørgensen KA. Acta Chem. Scand. 1996; 50:652–660.
6. Broggini G, Molteni G, Terraneo A, Zecchi G. Heterocycles. 2003; 59:823–858.
7. Boz E, Tüzün NŞ. J. Organomet. Chem. 2013; 724:167–176.
8. Jørgensen, KA. Cycloaddition reactions in organic synthesis. John Wiley & Sons; 2002.
9. Frühauf H-W. Coord. Chem. Rev. 2002; 230:79–96.
10. Walker JA, Knobler CB, Hawthorne MF. J. Am. Chem. Soc. 1983; 105:3370–3371.
11. Chetcuti PA, Walker JA, Knobler CB, Hawthorne MF. Organometallics. 1988; 7:641–650.
12. Chetcuti PA, Knobler CB, Hawthorne MF. Organometallics. 1988; 7:650–660.
13. Bühl M, Hnyk D, Macháček J. Chem. - Eur. J. 2005; 11:4109–4120. [PubMed: 15861374]
14. Bühl M, Hnyk D, Macháček J. Inorg. Chem. 2007; 46:1771–777. [PubMed: 17253682]
15. Bühl M, Holub J, Hnyk D, Macháček J. Organometallics. 2006; 25:2173–2181.
16. Hawthorne MF, Zink JI, Skelton JM, Bayer MJ, Liu C, Livshits E, Baer R, Neuhauser D. Science. 2004; 303:1849–1851. [PubMed: 15031500]
17. Pitochelli AR, Hawthorne FM. J. Am. Chem. Soc. 1960; 82:3228–3229.
18. Spokoyny AM. Pure Appl. Chem. 2013; 85:903–919.
19. Viñas C, Gomez S, Bertran J, Teixidor F, Dozol J-F, Rouquette H. Inorg. Chem. 1998; 37:3640–3643. [PubMed: 11670456]
20. Yinghuai Z, Hosmane NS. J. Organomet. Chem. 2013; 747:25–29.
21. Grüner B, Mikulášek L, Báča J, Císařová I, Böhmer V, Danila C, Reinoso-García MM, Verboom W, Reinhoudt DN, Casnati A, Ungaro R. Eur. J. Org. Chem. 2005; 2005:2022–2039.
22. Grüner B, Plešek J, Báča J, Císařová I, Dozol JF, Rouquette H, Viňas C, Selucký P, Rais J. New J. Chem. 2002; 26:1519–1527.
23. Barry NP, Sadler PJ. Chem. Soc. Rev. 2012; 41:3264–3279. [PubMed: 22307021]
24. Becke AD. J. Chem. Phys. 1993; 98:5648–5652.
25. Grimme S. J. Chem. Phys. 2006; 124:034108. [PubMed: 16438568]
26. Marenich AV, Cramer CJ, Truhlar DG. J. Phys. Chem. B. 2009; 113:6378–6396. [PubMed: 19366259]
27. Gonzalez C, Schlegel HB. J. Phys. Chem. 1990; 94:5523–5527.
28. Zhao Y, Truhlar DG. Theor. Chem. Acc. 2008; 120:215–241.
29. Wiberg KB. Tetrahedron. 1968; 24:1083–1096.
30. Foster JP, Weinhold F. J. Am. Chem. Soc. 1980; 102:7211–7218.
31. Frisch, MJ., Trucks, GW., Schlegel, HB., Scuseria, GE., Robb, MA., Cheeseman, JR., Scalmani, G., Barone, V., Mennucci, B., Petersson, GA., Nakatsuji, H., Caricato, M., Li, X., Hratchian, HP., Izmaylov, AF., Bloino, J., Zheng, G., Sonnenberg, JL., Hada, M., Ehara, M., Toyota, K., Fukuda,

R., Hasegawa, J., Ishida, M., Nakajima, T., Honda, Y., Kitao, O., Nakai, H., Vreven, T., Montgomery, JA., Jr, Peralta, JE., Ogliaro, F., Bearpark, M., Heyd, JJ., Brothers, E., Kudin, KN., Staroverov, VN., Kobayashi, R., Normand, J., Raghavachari, K., Rendell, A., Burant, JC., Iyengar, SS., Tomasi, J., Cossi, M., Rega, N., Millam, JM., Klene, M., Knox, JE., Cross, JB., Bakken, V., Adamo, C., Jaramillo, J., Gomperts, R., Stratmann, RE., Yazyev, O., Austin, AJ., Cammi, R., Pomelli, C., Ochterski, JW., Martin, RL., Morokuma, K., Zakrzewski, VG., Voth, GA., Salvador, P., Dannenberg, JJ., Dapprich, S., Daniels, AD., Farkas, O., Foresman, JB., Ortiz, JV., Cioslowski, J., Fox, DJ. Gaussian 09. Gaussian, Inc.; Wallingford, CT: 2009.

32. Legault, CY. 10b. Université de Sherbrooke; 2009. http://www.cylview.org
33. Krause H, Ernstberger B, Neusser H. Chem. Phys. Lett. 1991; 184:411–417.
34. Easter DC, Terrell DA, Roof JA. J. Phys. Chem. A. 2005; 109:673–689. [PubMed: 16833394]
35. Engkvist O, Hobza P, Selzle H, Schlag E. J. Chem. Phys. 1999; 110:5758–5762.
36. Tauer TP, Sherrill CD. J. Phys. Chem. A. 2005; 109:10475–10478. [PubMed: 16834301]
37. Lanzarotti E, Biekofsky RR, Estrin DA, Marti MA, Turjanski AG. J. Chem. Inf. Model. 2011; 51:1623–1633. [PubMed: 21662246]
38. Gonzalez C, Lim EC. J. Phys. Chem. A. 2001; 105:1904–1908.
39. Zhao Y, Truhlar DG. Acc. Chem. Res. 2008; 41:157–167. [PubMed: 18186612]
40. Cramer CJ, Truhlar DG. Phys. Chem. Chem. Phys. 2009; 11:10757–10816. [PubMed: 19924312]
41. Liu F, Paton RS, Kim S, Liang Y, Houk KN. J. Am. Chem. Soc. 2013; 135:15642–15649. [PubMed: 24044412]
42. Ess DH, Houk KN. J. Am. Chem. Soc. 2007; 129:10646–10647. [PubMed: 17685614]
43. Fernández I, Cossío FP, Bickelhaupt FM. J. Org. Chem. 2011; 76:2310–2314. [PubMed: 21388217]
44. Lan Y, Wheeler SE, Houk KN. J. Chem. Theory Comput. 2011; 7:2104–2111. [PubMed: 26606482]
45. Fernández I, Bickelhaupt FM. J. Comput. Chem. 2012; 33:509–516. [PubMed: 22144106]
46. Gordon CG, Mackey JL, Jewett JC, Sletten EM, Houk KN, Bertozzi CR. J. Am. Chem. Soc. 2012; 134:9199–9208. [PubMed: 22553995]
47. Liang Y, Mackey JL, Lopez SA, Liu F, Houk KN. J. Am. Chem. Soc. 2012; 134:17904–17907. [PubMed: 23061442]
48. Fernández I, Bickelhaupt FM, Cossío FP. Chem. - Eur. J. 2012; 18:12395–12403. [PubMed: 22915249]
49. Lopez SA, Houk KN. J. Org. Chem. 2013; 78:1778–1783. [PubMed: 22764840]
50. Fernández I, Solà M, Bickelhaupt FM. Chem. - Eur. J. 2013; 19:7416–7422. [PubMed: 23576307]
51. Ess DH, Houk KN. J. Am. Chem. Soc. 2008; 130:10187–10198. [PubMed: 18613669]
52. Chetcuti PA, Hawthorne MF. J. Am. Chem. Soc. 1987; 109:942–943.

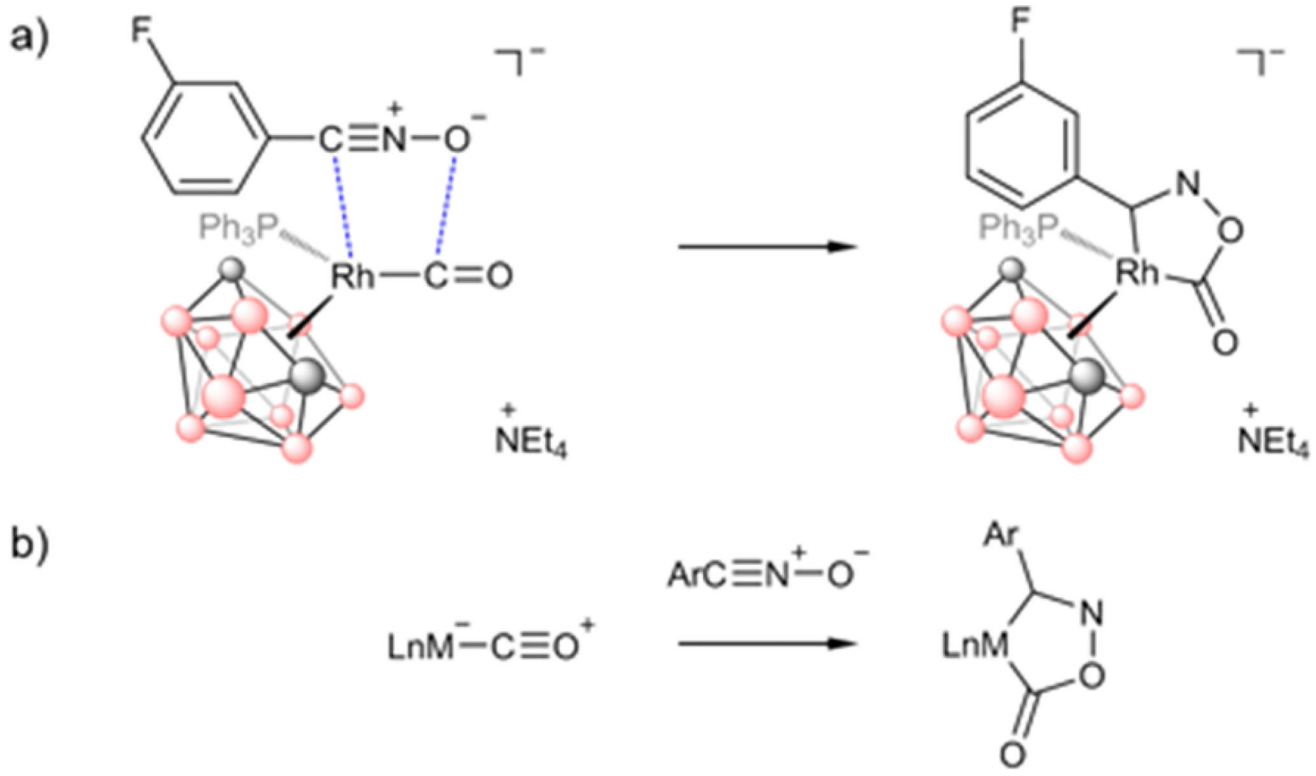

Figure 1.

(a) First 1,3-dipolar cycloaddition to polarized metal–carbon bonds between *m*-fluorobenzonitrile *N*-oxide and rhodacarborane anion $[Rh(PPh_3)(CO)(C_2B_9H_{11})]^-$. The carborane, $C_2B_9H_{11}$, is represented with balls and sticks, where B is in pink and C is in black.[10] (b) Generic arylnitrile oxide cycloaddition to metal–CO bonds.

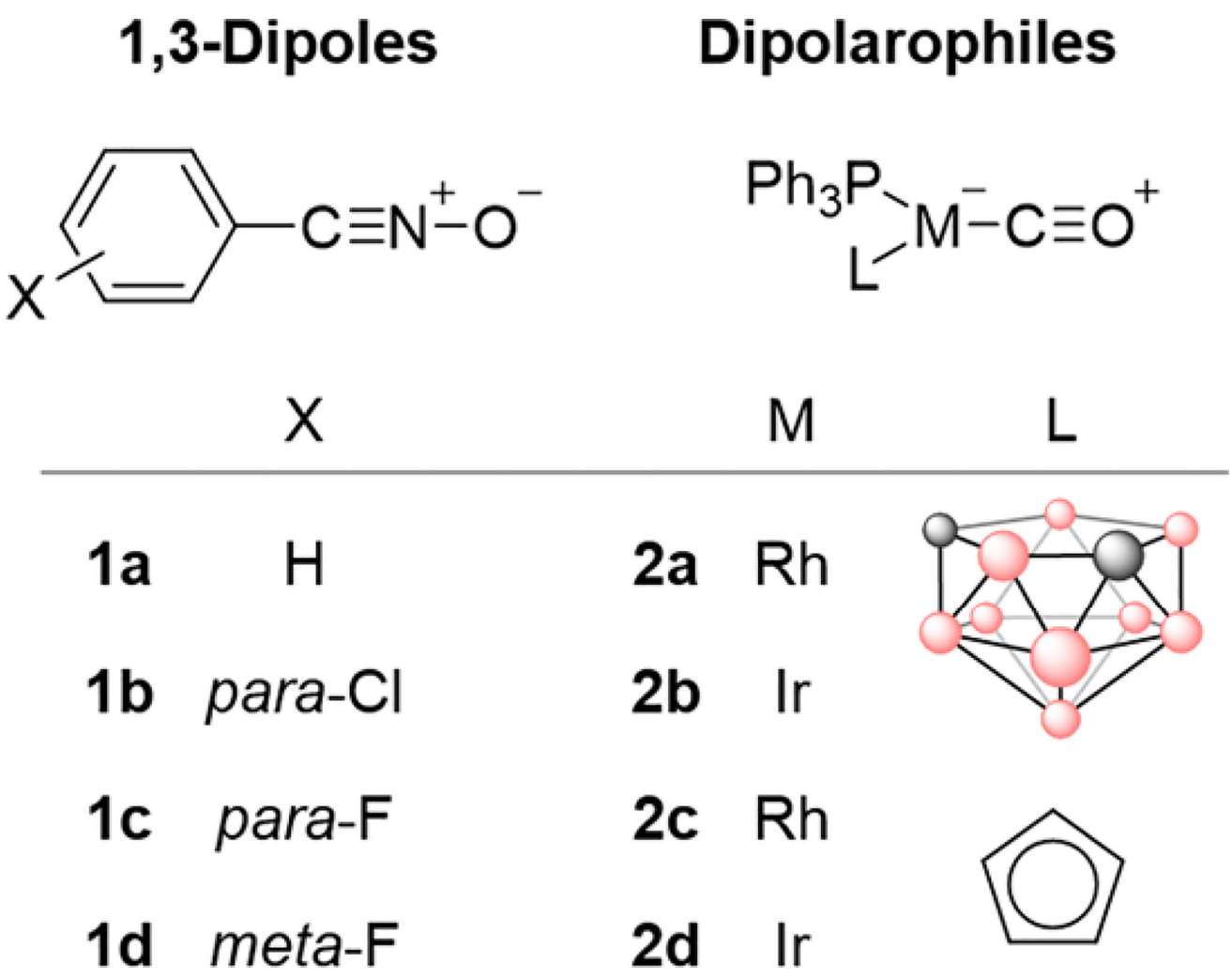

Figure 2.

1,3-Dipoles and dipolarophiles modeled in the present study. The carboranyl ligand, $(C_2B_9H_{11})^{2-}$, is represented with balls and sticks, where B is in pink and C is in black.

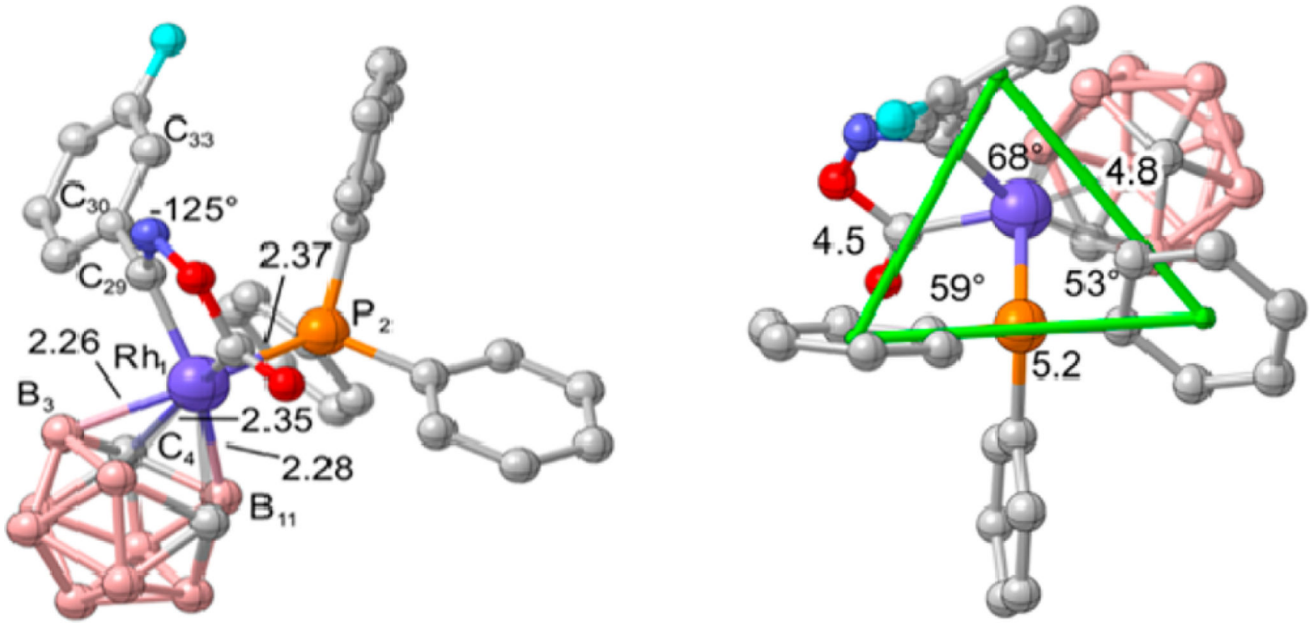

Figure 3.

B3LYP-D3 optimized structure of the metallacycle product **1d–2a** shown in two different orientations. The color scheme is C in gray, O in red, P in orange, B in pink, F in cyan, and Rh in purple. H atoms are omitted for clarity. The green triangle represents the distances between the centers of the fluorobenzene ring and two of the phenyls of the triphenylphosphine. Distances are shown in Angstrom and angles in degrees.

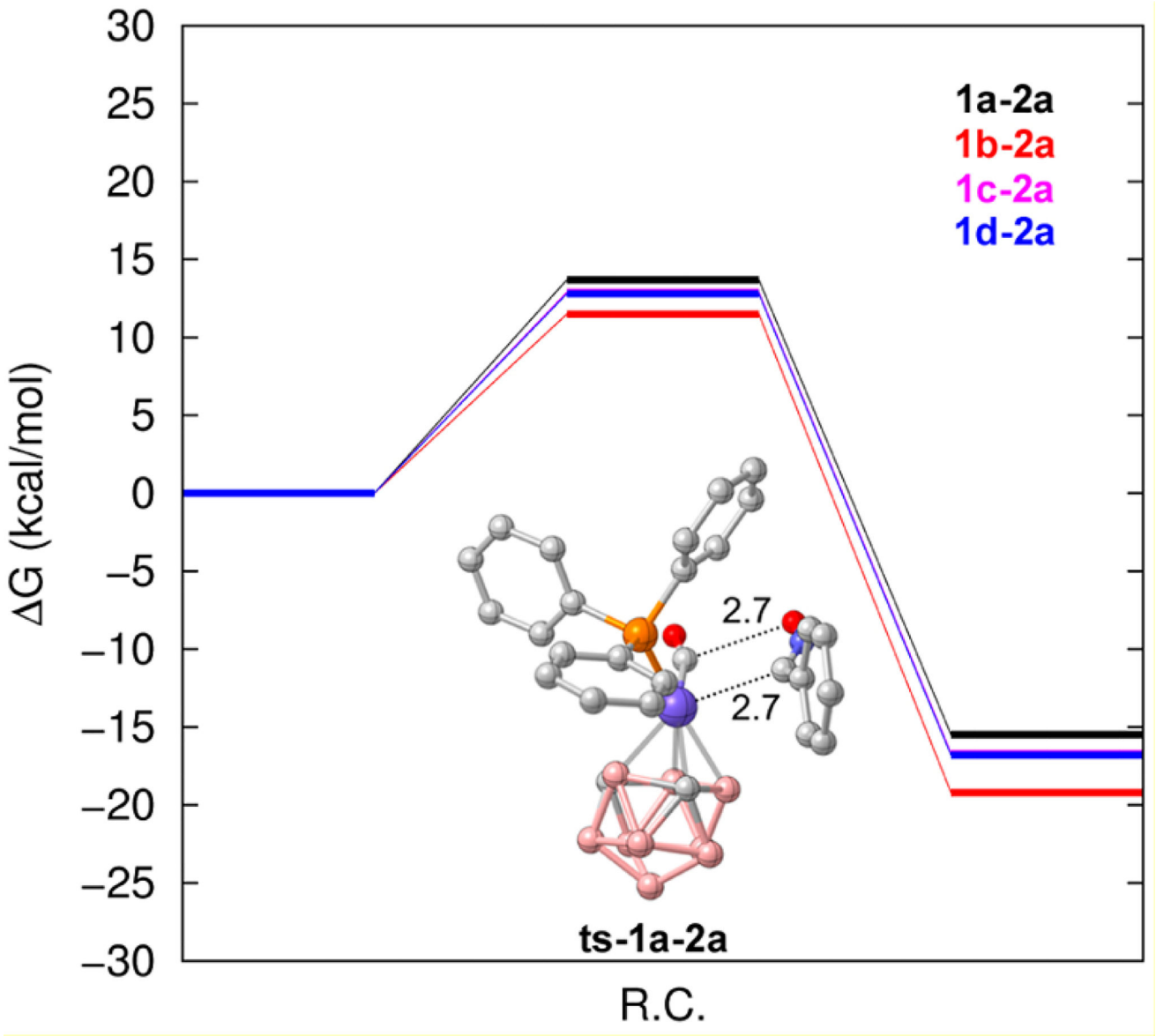

Figure 4.

Plot of activation and reaction free energies for the reactions between dipolarophile **2a** and 1,3-dipoles **1a–d**, calculated with M06//B3LYP-D3/6-31G(d)+SDD(Rh,Ir). Energies are given in kcal mol^{-1}. The optimized structure of **ts-1a-2a** is shown as an inset with the following colors; C in gray, O in red, P in orange, B in pink, and Rh in purple. R.C. means reaction coordinate.

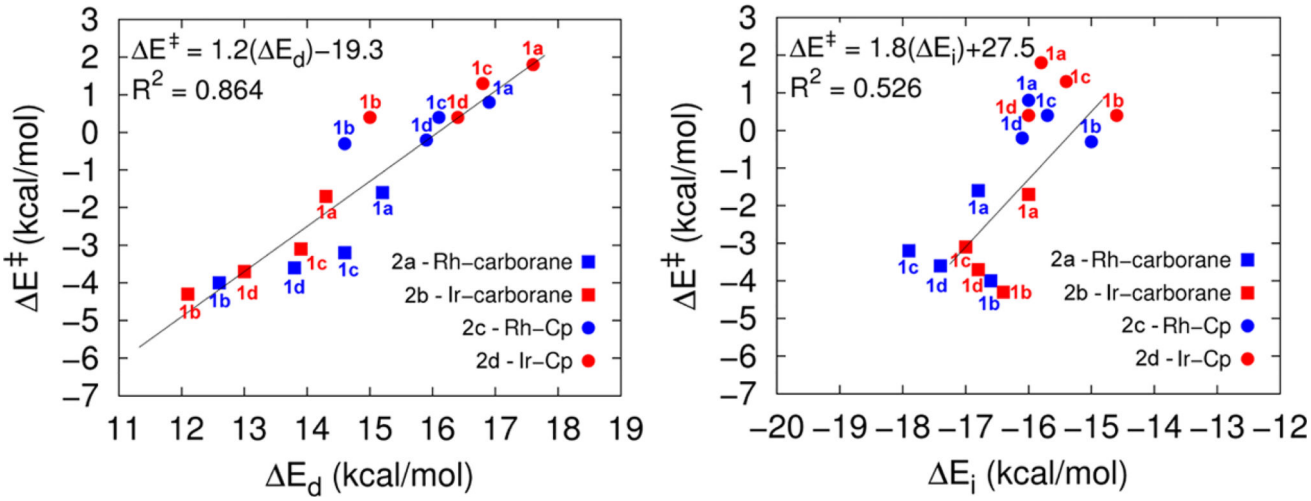

Figure 5.

Activation energies ($\Delta E^{\ddagger}$) versus distortion energies (ΔE_d, left panel) and interaction energies (ΔE_i, right panel) calculated with M06//B3LYP-D3/6-31G(d)+SDD(Rh,Ir).

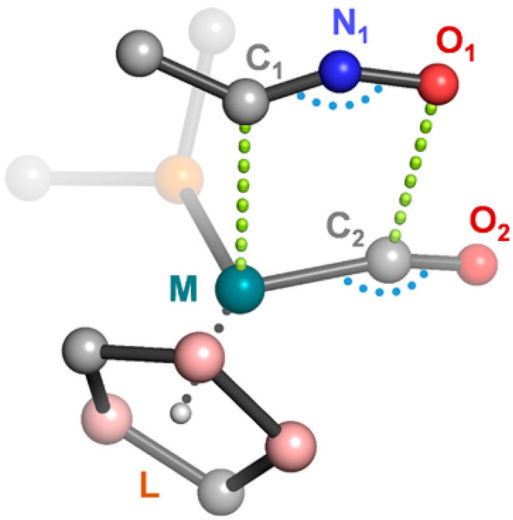

	ts-1d-2a	ts-1d-2b	ts-1d-2c	ts-1d-2d
M	Rh	Ir	Rh	Ir
L	$(C_2B_9H_{11})^{2-}$	$(C_2B_9H_{11})^{2-}$	$(C_5H_5)^-$	$(C_5H_5)^-$
$\Delta G^{\ddagger}$	12.8	12	16.8	17.4
ΔG_r	-16.8	-25.5	-11.7	-19.8
$M–C_1$	2.76	2.82	2.61	2.66
$C_2–O_1$	2.79	2.92	2.63	2.73
$M–C_2$	1.87	1.86	1.88	1.86
$C_2–O_2$	1.16	1.17	1.16	1.16
$C_1–N_1$	1.21	1.21	1.22	1.22
$N_1–O_1$	1.24	1.24	1.24	1.24
$M–C_2–O_2$	162	167	163	168
$C_1–N_1–O_1$	150	150	145	144

Figure 6.

Transition structures for the 1,3-dipolar cycloaddition of arylnitrile *N*-oxide **1d** and Rh(I)/Ir(I) complexes **2a–d**, calculated with M06//B3LYP-D3/6-31G(d)+SDD(Rh,Ir). Distances are shown in Angstrom and angles in degrees. Aryl groups and most of the carboranyl ligands have been omitted for clarity. Activation ($\Delta G^{\ddagger}$) and reaction energies (ΔG_r) are given in kcal mol^{-1}.

Table 1

Gibbs Free Activation Energy ($\Delta G^{\ddagger}$), Reaction Free Energy (ΔG_r), Reaction Enthalpy (ΔH), Entropy ($T{\cdot}\Delta S$, Calculated at 298 K), and Charge Transfer (CT) at the Metal Atoms (Rh and Ir) Calculated with M06//B3LYP-D3/6-31G(d)+SDD(Rh,Ir)[a]

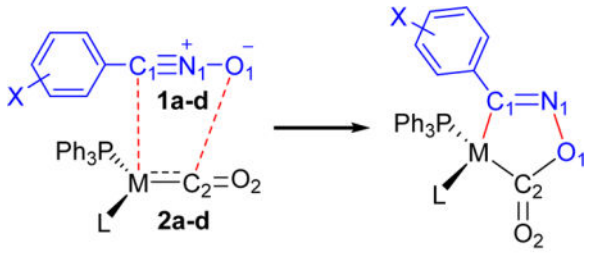

X		M	L
1a	H	**2a**	Rh
1b	*para*-Cl	**2b**	Ir
1c	*para*-F	**2c**	Rh
1d	*meta*-F	**2d**	Ir

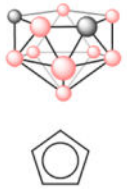

reaction	$\Delta G^{\ddagger}$	ΔG_r	ΔH	$-T{\cdot}\Delta S$	CT
2a + 1a	13.7	−15.5	−33.3	17.7	0.16
2a + 1b	11.5	−19.2	−36.7	17.5	0.18
2a + 1c	12.9	−16.7	−35.0	18.3	0.18
2a + 1d	12.8	−16.8	−36.0	19.2	0.23
2b + 1a	14.1	−23.7	−41.9	18.2	0.16
2b + 1b	12.6	−26.7	−46.0	19.3	0.19
2b + 1c	12.9	−25.2	−43.7	18.5	0.19
2b + 1d	12.0	−25.5	−44.5	19.0	0.23
2c + 1a	16.1	−11.1	−29.2	18.0	0.16
2c + 1b	16.8	−11.8	−30.3	18.5	0.18
2c + 1c	16.1	−11.3	−30.5	19.1	0.18
2c + 1d	16.8	−11.7	−30.7	19.0	0.22

reaction	$\Delta G^{\ddagger}$	ΔG_r	ΔH	$-T\Delta S$	CT
2d + 1a	15.5	−18.6	−36.0	17.4	0.16
2d + 1b	16.4	−19.9	−37.3	17.5	0.18
2d + 1c	16.5	−18.9	−36.5	17.6	0.19
2d + 1d	17.4	−19.8	−38.1	18.3	0.23

[a] Energies are in kcal mol^{-1}.

Table 2

Selected Wiberg Bond Indices Calculated via NBO Analysis for the Reactants (2a and 1d), Transition State (ts-1d-2a), and Product (1d–2a)[a]

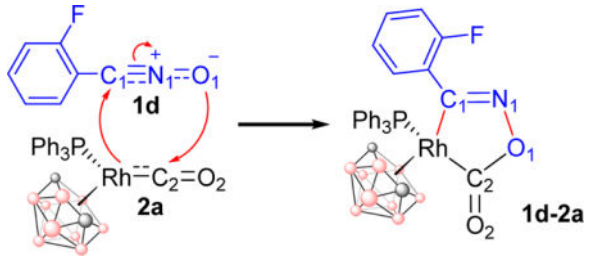

compound	Rh–C_2 (C–C)	C_1–N_1	N_1–O_1	Rh–C_1 (C–C_1)	C_2–O_1 (C–O_1)
1d		2.3	1.5		
2a	1.2 (2.0)				
ts-1d-2a	1.1 (1.7)	2.1 (2.1)	1.4 (1.4)	0.2 (0.3)	0.0 (0.2)
1d–2a	0.7 (1.0)	1.8 (1.8)	1.0 (1.0)	0.7 (1.0)	0.9 (0.9)

[a] As a reference, the numbers in parentheses correspond to the reaction between ethylene and **1d**.